Journal of Cultural Heritage 61 (2023) 1–12

Contents lists available at ScienceDirect

Journal of Cultural Heritage

journal homepage: www.elsevier.com/locate/culher

Original article

Numerical modelling-based damage diagnostics in cultural heritage structures

A.M. D'Altri[a,b,*], S. de Miranda[a], G. Castellazzi[a], B. Glisic[b]

[a] Department of Civil, Chemical, Environmental, and Materials Engineering, University of Bologna, Italy
[b] Department of Civil and Environmental Engineering, Princeton University, USA

ARTICLE INFO

Article history:
Received 24 June 2022
Accepted 15 February 2023
Available online 28 February 2023

Keywords:
Mesh generation
Masonry cracking
Damage scenario
Historical masonry structure
Point cloud-to-numerical model
Virtual tour

ABSTRACT

In this paper, a numerical modelling-based damage diagnostics methodology is proposed for cultural heritage structures (CHSs) made of masonry. Firstly, an integration of 3D documentation data (i.e. point clouds and virtual tours) is developed for the rapid numerical model generation of CHSs. This allows to directly exploit non-comprehensive point clouds (e.g., associated to outer surfaces only) for the solid finite element model generation, where the lacking information is merged with off-site interactive and immersive frameworks. Secondly, a number of nonlinear static and dynamic analyses are conducted on the generated solid model to account for various load scenarios (e.g., earthquakes, soil settlements, etc.), considering a nonlinear continuum constitutive law. Thirdly, a crack pattern matching indicator is introduced to quantitatively identify the most likely load scenario which originated the damage pattern present in the CHS, by comparing numerical and actual crack patterns. The proposed methodology allows to rapidly generate and extract the numerical model that reflects the current (damaged) state of the CHS. This also allows to identify the parts of the CHS susceptible to further damage. The effectiveness of the proposed methodology is promisingly assessed on an actual historical masonry structure, the Morris Island lighthouse in South Carolina (USA).

1. Introduction

Cultural heritage structures (CHSs), such as palaces, fortresses, mosques, churches, lighthouses, castles, etc., mostly made of masonry, represent a considerable portion of the world heritage [1]. Accordingly, CHSs conservation is of primary importance to guarantee CHSs survival to next generations.

The first task towards CHSs conservation consists in acquiring an accurate knowledge of the CHSs. This task is already very challenging given the complex evolution of CHSs along the centuries, characterized by several impacting events such as repairs, modifications, demolitions and reconstructions, earthquakes, foundation settlements, shelling, materials ageing, thermal effects, etc. These events could have induced cracking in historical masonries, which result in complex crack patterns whose interpretation is typically arduous [2–4].

The diagnostic process, which attempts to interpret how crack patterns may have originated on CHSs (i.e., the causes of damage), is of primary importance to the knowledge of the CHS [5,6]. Indeed, damage diagnostics is essential and preparatory to optimally design structural health monitoring (SHM) systems [7–9] and to reliably assess the structural performance of the CHS [10,11].

It should be stressed that the actual crack pattern of the CHS has to be known to perform damage diagnostics. The actual crack pattern in CHSs is typically obtained through visual damage surveys [12]. When the whole crack pattern cannot be inspected visually, damage identification procedures, such as [13,14], could be used to localize and quantify damage on CHSs.

Given the complex geometries and the nonlinear structural behaviour of CHSs, their structural assessment is generally undertaken through advanced numerical modelling strategies [15]. Three main families of modelling strategies can be distinguished for masonry structures: (i) block-based models [16–18], where each block of the structure is explicitly modelled, (ii) continuum models [19–21], where an equivalent fictitious homogeneous continuum is used for masonry, (iii) geometry-based models [22–25], where the structure is modelled as a rigid body typically employing limit analysis solutions. Nowadays, although geometry-based models appear appealing for the analysis of domes and vaulted structures (and macro-block limit analysis based on observed damage may provide satisfactory results when dealing with seismic actions [25]), continuum modelling appears the most efficient modelling strategy for CHSs, given the capability to deal with complex

* Corresponding author.
E-mail address: am.daltri@unibo.it (A.M. D'Altri).

https://doi.org/10.1016/j.culher.2023.02.004

large-scale structures with a feasible computational demand [15]. To this regard, many nonlinear constitutive continuum models, based either on fracture mechanics, damage mechanics, or plasticity theory, have been lately utilized for masonry and historical structures [15].

From the pioneering work of Mastrodicasa [2] based on empirical evidence to relate crack patterns to foundation settlements, recent advancements in crack diagnostics employed numerical techniques. Although many numerical strategies have been lately proposed for historical masonry structures, few approaches have been specifically developed to deal with damage diagnostics.

Mostly, qualitative comparisons of the actual crack pattern to the results of numerical analyses can be found in the literature [26]. For example, the identification of the causes of damage in the Church of the Nativity in Bethlehem has been carried out in [27] by means of a nonlinear continuum 3D approach. In [28], the damage assessment of an Italian medieval castle has been performed through a continuum modelling approach to account for foundation settlements. Furthermore, the origin of cracks in double-wall industrial masonry chimneys (due to thermal effects) has been investigated in [12] by using the extended finite element method, as well as an isotropic continuum approach.

To the best of the authors' knowledge, only a very few examples of quantitative damage diagnostics approaches can be found in the literature. Among these, a quantitative methodology for diagnosing crack patterns in masonry structures using photogrammetry and distinct element modelling has been originally developed in [29], with an application to a foundation wall in the Baptistery of San Giovani in Florence, Italy. Such idea has been more recently coupled with an automated data-driven procedure in [30] to speed-up the identification process for settlement-induced cracking.

Another well-known challenge that arises when dealing with numerical modelling of CHSs is the generation of the geometrical model. Indeed, CHSs often show complex and irregular geometries, leading to time-consuming tasks. To address this issue, few point cloud-to-numerical model techniques have been lately developed [31–34] to attempt to exploit point clouds (typically surveyed on CHSs for documentation purposes [35]) to aid the generation of the numerical model.

In this paper, a general quantitative methodology for damage diagnostics in cultural heritage masonry structures based on continuum modelling is proposed and tested on an actual CHS. To this aim, two main novelties are introduced.

The first one consists in the integration of 3D documentation data (i.e. point clouds and virtual tours) for the rapid numerical model generation of CHSs. Basically, this represents the extension of a point cloud-to-numerical model procedure (Cloud2FEM [34,36,37]) to deal with non-comprehensive point clouds (for example associated to outer surfaces only, which is the most common case in real applications). Particularly, the lacking information is merged with off-site interactive and immersive frameworks.

The second one consists in the introduction of a crack pattern matching indicator to quantitatively identify the most likely load scenario which originated the damage pattern present in the CHS, by comparing numerical and actual crack patterns.

This paper is structured as follows. Section 2 summarizes the research aim of the paper. Section 3 discusses the point cloud-to-numerical modelling and the damage diagnostics methodology. Section 4 shows and discusses the results obtained on an actual CHS. Section 5 summarizes the main conclusions of this research work.

2. Research aim

The aim of this paper is to propose a general quantitative methodology for damage diagnostics in cultural heritage masonry structures based on numerical modelling. The methodology is able to identify the most likely load scenario which originated the damage pattern present in the CHS. To achieve this aim, two main tasks are developed. The first concerns the rapid generation of the CHS numerical model from point clouds (supported by virtual tours), while the second concerns the extraction of the model that reflects the current damaged state of the CHS.

More in detail, an integration with virtual tours is firstly introduced to deal with non-comprehensive point clouds for the generation of a consistent solid Finite Element (FE) model. Secondly, a crack pattern matching indicator, based on the comparison of numerical and actual crack patterns, is introduced to quantitatively identify the most likely load scenario which originated the damage pattern present in the CHS, after the conduction of a number of nonlinear static and dynamic analyses on the generated model.

The effectiveness of the methodology is assessed on an actual historical masonry structure, the Morris Island lighthouse in South Carolina (USA).

3. Materials and methods

In this section, the CHS used to assess the methodology is firstly introduced to ease the presentation. Then, the point cloud-to-numerical modelling framework is detailed. Finally, the methodology for damage diagnostics is formulated.

3.1. Morris Island lighthouse

Three different masonry lighthouses were subsequently built on Morris Island. A first permanent lighthouse was built from 1757 to 1777 and it was completely destroyed by fire. Then, a second lighthouse (an octagonal brick tower) located further South on Morris Island was constructed in 1801. This lighthouse served the Charleston harbour until 1860, and it was completely destroyed in the American Civil War to impair navigation to Charleston's harbour. After the war, a new masonry lighthouse (the current one) was constructed in 1876 as a symbol of federal strength [38]. The current lighthouse has a circular cross-section (base and top diameters about 8.0 m and 4.5 m, respectively) and several openings located on the same radial plane. The structure decreases in thickness while approaching the top. The wall thickness at the bottom is about 1.15 m, which is composed of 8 interconnected clay brick layers with Flemish bond.

The 1886 Charleston earthquake (6.7–7.1 magnitude [39] with an estimated peak ground acceleration equal to 0.33 g [40]) induced two large cracks in the masonry structure (which were never repaired [38]). In 1938, the lighthouse was abandoned as a jetty system involuntarily induced the erosion of Morris Island [38], which also induced the structure to lean. Then, an automatic beacon was installed, and the lighthouse remained in commission until 1962 [41].

Presently, the non-profit organization Save the Light, Inc. [42] manages the historical structure aiming at preserving it [41]. This CHS is persistently threated by salt spray, high winds, biological degradation by sea birds, and foundation settlements, as well as potential future hurricanes and earthquakes [41]. The Morris Island lighthouse is used in this research to assess the effectiveness of the methodology proposed in this paper.

3.2. Point cloud-to-numerical modelling

In this section, the rapid generation of the numerical model of a CHS from point clouds is shown and discussed. The Cloud2FEM procedure developed by Castellazzi et al. [34,36,37] is here employed.

Such workflow semi-automatically exploits dense point clouds to generate solid FE models. Particularly, a fully comprehensive point cloud (i.e., comprising inner and outer surfaces of the structure) is firstly sliced over the vertical direction. Then, closed polylines are automatically extracted on each slice by connecting representative points of the inner and outer borders. Thanks to the automatic classification of inner and outer polylines developed in [43], their subtraction gives directly closed polygons. Each slice is digitalized, i.e., transformed into pixels with a certain resolution, and stacked vertically generating a 3D object made of voxels. Finally, voxels are transformed into 8-node hexahedral elements, and a conforming 3D solid FE mesh is obtained. For more details, the interested reader is referred to [34,36,37].

It is important to emphasize that if the point cloud does not include the inner surfaces of the structure, as it often occurs in complex CHSs due to budget limitations (and it is the case of Morris Island lighthouse), the aforementioned workflow lacks information to reliably generate a FE model. Accordingly, integration with off-site interactive and immersive frameworks (i.e., virtual tours), which are increasingly utilized in CHS for documentation purposes [44,45], is herein originally introduced to deal also with non-comprehensive point clouds.

Virtual tour environments made by spherical panoramas [44] are an appealing alternative to gather indoor data, as they are typically less expensive and faster to perform than laser scanner/photogrammetric surveys. Even though virtual tours do not generally provide quantitative geometric information, their qualitative contribution appears sufficient to generate consistent FE models. Indeed, the possibility of the user to off-line inspect the inner parts of the structure while creating the slices is essential in most practical cases, e.g. in presence of shafts, wall openings, thickness walls irregularities, non-structural parts, debris, furniture, etc. This can be further eased when the virtual tour is organized through hotspots (see e.g., [41]), so that the user can follow the slices creation by virtually moving within the structure. Finally, the integration with virtual tour environments is straightforwardly facilitated by the graphical tools (i.e., offsetting, adding, moving, removing, joining of polylines) lately developed in the open source Cloud2FEM software [37].

It should be pointed out that the point cloud data related to non-structural parts should be cleaned in order to guarantee the generation of a suitable model for structural purposes. To this aim, the point cloud cleaning, that is typically a manual operation, can be conducted either a priori on the 3D point cloud (i.e., prior to the slicing operation) or directly into the Cloud2FEM software [37] at the 2D slice level. Once the point cloud is cleaned from non-structural parts, it can be used to generate the 3D solid FE mesh. Indeed, the intrinsic error (noise) of the surveying technique (laser scanning or photogrammetry) is typically one order of magnitude lower than the accuracy needed in the 3D FE model, and hence it can be neglected.

An example of point cloud-to-numerical modelling with non-comprehensive point cloud and virtual tour integration is given in Fig. 1 for the Morris Island lighthouse. In particular, Fig. 1 shows: the point cloud of the lighthouse, externally-only acquired as specified in [41]; the slicing of the point cloud with 0.4 m steps (102 slices in total), where the internal geometry has been semi-automatically reconstructed with the support of the virtual tour through graphical tools (e.g. offsetting and joining of polylines [37]); an example of integration of the lacking information at the slice level (slice 49); the virtual tour environment organized through hotspots [41], where an example of non-structural part that can be inspected by means of the virtual tour and taken into account into the slices is also shown; the resulting "Voxel model", obtained by adopting a 0.4 × 0.4 m plan grid. It should be pointed out that the choice of the voxel size (0.4 × 0.4 × 0.4 m) has been here adopted in agreement with the suggestions given in [34,36,46], where the adoption of the voxel size based on the dimension of structural details (e.g. openings) and/or on the geometrical irregularity of the structure is suggested. In order to assess the effectiveness of the Voxel model and to verify its geometry, a total volume-invariant smoothing operation has been conducted on the bounding surfaces of the Voxel model. The resulting watertight mesh made of triangles has been filled with tetrahedrons, obtaining the "Smooth model", see Fig. 1. The Voxel model validation is shown and discussed in Section 4.1.

3.3. A methodology for damage diagnostics

In this section, the methodology for damage diagnostics is presented. The solid continuum FE model generated according to the workflow described in previous section is employed.

In the following, a homogeneous isotropic plastic-damaging 3D continuum [47], based on tensile and compressive damage scalar variables, is assumed for masonry (Section 3.3.1). Then, the crack pattern matching indicator (Section 3.3.3) is formulated considering the tensile damage variable, which indicates material cracking. Of course, the damage diagnostics methodology herein presented remains valid for any suitable nonlinear constitutive law for quasi-brittle materials while adopting the appropriate variable that indicates material cracking.

3.3.1. Material constitutive law

Here, the isotropic continuum plastic-damage material behaviour based on the model proposed by Lee and Fenves [47] is adopted. It considers tensile and compressive responses governed by two independent damage variables (i.e., tensile damage $0 \le d_t < 1$, and compressive damage $0 \le d_c < 1$). Consequently, the uniaxial stress-strain relationships can be represented by:

$$\sigma_t = (1-d_t)E\left(\varepsilon_t - \varepsilon_t^p\right),$$
$$\sigma_c = (1-d_c)E\left(\varepsilon_c - \varepsilon_c^p\right), \quad (1)$$

where σ_t is the uniaxial tensile stress, σ_c is the uniaxial compressive stress, E is the material Young's modulus, ε_t and ε_c are the uniaxial tensile and compressive strains, and ε_t^p and ε_c^p are the uniaxial tensile and compressive plastic strains.

Two main limitations on the usage of this model for masonry can be observed:

- *Isotropic response*. Generally, masonry shows an anisotropic behaviour at pre-peak, peak, and post-peak responses. However, the mechanical characterization of anisotropic continua can be a very challenging task due to the many parameters that need definition, as well as the fact that masonry mechanical characterization is typically very poor in historical buildings due to budget limitations and restrictions for destructive testing. While this aspect has a significant role at the small-scale specimen level, it is less impacting at the large-scale level of CHSs, where multi-leaf very thick masonries are typically found. Indeed, it appears reasonable to think that the anisotropic nature of the masonry material will be more significant in single-layer walls rather than in very thick walls (which will plausibly tend to a more isotropic response). Additionally, it should be stressed that the tensile strength of the homogeneous continuum is a fictitious material property which attempts to describe the material behaviour in tension. This is an intrinsic limitation of continuum models. For this reason, tensile strength is typically calibrated or used as varying quantity in parametrical analyses. Nonetheless, the isotropic plastic-damage model herein considered has been extensively tested for masonry and compared with other modelling approaches (e.g., in [48,49]), confirming

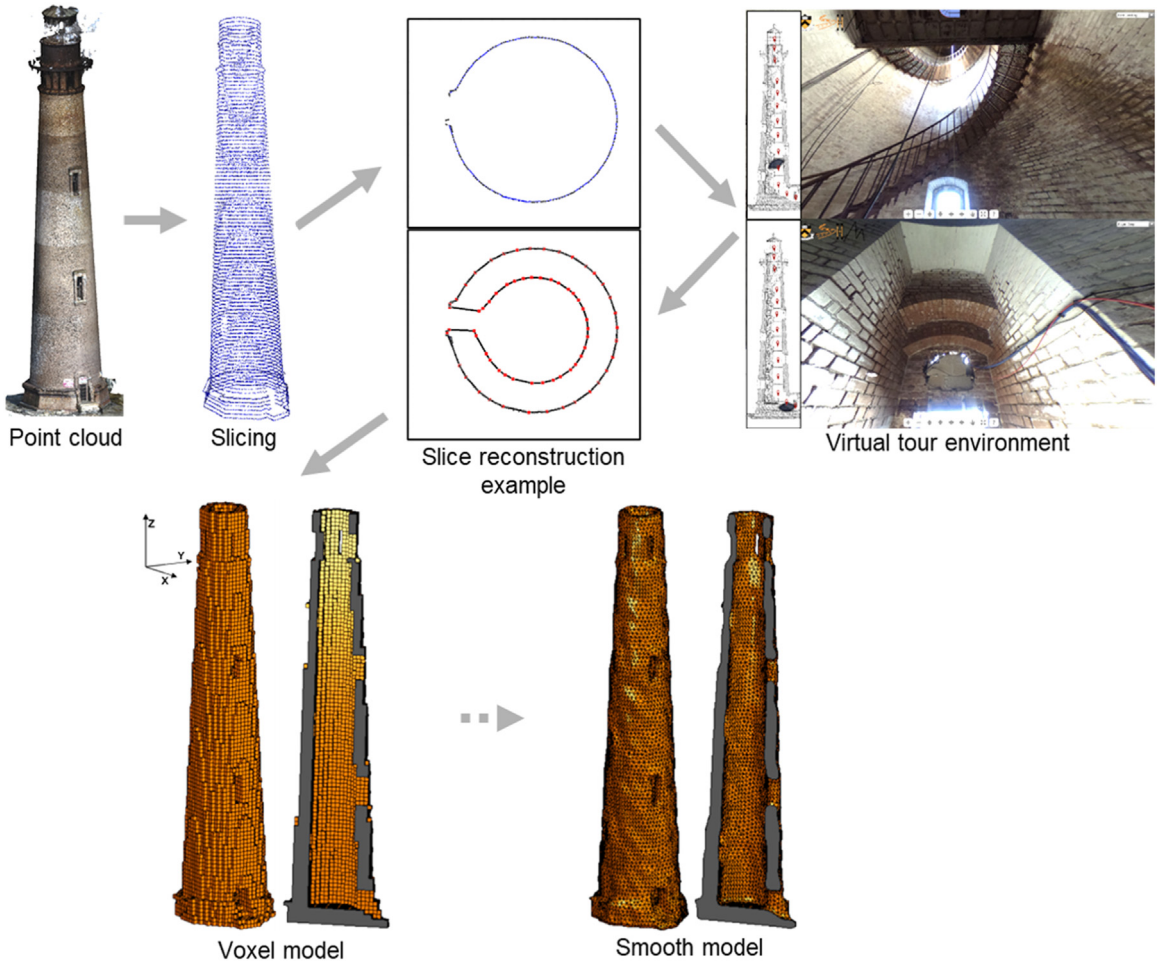

Fig. 1. Point cloud-to-numerical modelling of the Morris Island lighthouse based on Cloud2FEM software [37] and integration with virtual tour. From left: Point cloud of the exterior surfaces (from [41]); Slicing of the point cloud; Example of integration of missing (inner) information on a slice; Two screenshots of the virtual tour environment (from [41]); Resulting voxel model (12,410 8-node elements, total volume 794.24 m^3); Smooth model (92,942 4-node elements, total volume 794.28 m^3).

its ability to deal with both flexural and shear wall failures with the same mechanical set-up.

- *Plastic cyclic response*. Modelling the cycling response of masonry is another very challenging task. This becomes clear by observing that the rocking mechanism (flexural failure) in masonry walls is characterized by nearly-zero energy dissipation (i.e., no significant plastic deformations due to the cyclic opening and closuring of sub-horizontal cracks), whereas the shear failure is mainly governed by friction and is characterized by a significant energy dissipation (i.e., significant plastic deformations along the masonry joints) [50]. The isotropic plastic-damage model herein considered assumes crack opening as plastic deformation and a full stiffness recovery upon crack closure. Accordingly, this model appears not to be best suited to model rocking mechanisms of masonry walls. However, crack closure is typically nonperfect in large-scale CHSs given their multi-leaf very thick masonries (e.g., debris may fall in the cracks, preventing their closure), see for example the damage pattern of the CHS in [51]. With this in mind, the plastic cyclic response of the model herein considered appears sufficiently suitable for historical masonries in large-scale CHSs.

3.3.2. Load scenarios

A number of nonlinear static and/or dynamic analyses are conducted on the generated model to simulate the effects of several load scenarios. The choice of the load scenarios to be included in the study depends on the specific CHS, on its history, on its territorial hazards, and has to be carried out only after having reached a sufficient level of knowledge on the CHS. An example of load scenarios selection is shown and discussed in Sections 4.2-4.3.

3.3.3. Crack pattern matching indicator

A crack pattern matching indicator is here introduced to quantitatively identify the most likely load scenario which originated the damage pattern present in the CHS. Such indicator is based on the comparison between the actual crack pattern and numerical crack patterns, obtained in a number of nonlinear simulations.

Firstly, a definition of zones is performed on the generated FE model according to the actual crack pattern experienced by the CHS. In particular, the portions of the FE model where actual cracks are present are defined as "Fissure zone" through a set of elements, characterized by the volume V_F. Then, the rest of the FEs of the model are defined as "Intact zone", characterized by the volume V_I. This operation is especially facilitated by the rational arrangement of the Voxel model, which allows a simple and straightforward element set definition by the user. It should be herein anticipated that the definition of Fissure and Intact zones, that is carried out in agreement with the actual crack pattern of the CHS (that has to be known in detail), has a limited influence on the crack pattern matching indicator, as shown in the following (see Section 4.2.2).

Secondly, nonlinear simulations (accounting for the load scenarios defined in Section 3.3.2) are conducted. In the post-processing phase, the average tensile damage in the Fissure zone $\bar{d}_F$ and in the Intact zone $\bar{d}_I$ are computed for each load scenario as:

$$\bar{d}_F = \frac{1}{V_F}\int_{V_F} d_t \; dV_F \;,$$
$$\bar{d}_I = \frac{1}{V_I}\int_{V_I} d_t \; dV_I, \tag{2}$$

The crack pattern matching indicator ρ, which can be seen as a normalized distance between the average damage values in Fissure and Intact zones, is defined as:

$$\rho = \begin{cases} 0 \; with \; \bar{d}_F < \lambda \\ \frac{\bar{d}_F - \bar{d}_I}{\bar{d}_I} \; with \; \bar{d}_F \geq \lambda \end{cases} \tag{3}$$

where λ is a damage threshold specified by the user (in the present study $\lambda = 10\%$).

Note that, when the Fissure zone is not characterized by a significant damage level there is no interest in evaluating the crack pattern matching indicator. It should be also stressed that the case $\bar{d}_I = 0$, which would lead to a ρ with no meaning, does not occur in actual cases as shown in the following.

High values of ρ indicate a numerical crack pattern mainly characterized by tensile damage in the Fissure zone and a mostly undamaged Intact zone, i.e., a numerical crack pattern is in agreement with the actual one. Conversely, low values of ρ point out the origin of tensile damage in the Intact zone and/or a Fissure zone without significant damage, i.e., a numerical crack pattern is in disagreement with the actual one.

It should be highlighted that the value of ρ has a relative meaning, depending on the definition of zones. Once defined Fissure and Intact zones, the highest value of ρ will indicate the load scenario that best fits the actual crack pattern, i.e. the most likely load scenario which originated the damage pattern present in the CHS. The influence of the zone definition on the crack pattern matching indicator ρ is shown in Section 4.2.2.

Finally, it should be highlighted that, although the approach is based on a rapid generation of the FE model from point clouds and virtual tours, the definition of fissure and intact zones is manually conducted based on the knowledge of the current damaged state of the CHS. Nonetheless, the rational (voxel-based) discretization of the FE model allows a very straightforward assignation of fissure and intact zones.

4. Results and discussion

In this section, the outcomes of the Voxel model validation (Section 4.1), as well as the main results of the damage diagnostics methodology applied on the Morris Island lighthouse using nonlinear static (Section 4.2) and dynamic (Section 4.3) analyses are shown and discussed. The mechanical properties assumed for the masonry material are shown in the Appendix, parametrically adopting the material tensile strength f_t: 0.05, 0.08, 0.10, 0.15, and 0.20 MPa (denoted as ft050, ft080, ft010, ft015, ft020, respectively). It should be pointed out that, in preliminary analyses, the tensile strength value has been found to have a considerable influence on the crack pattern of the structure. For this reason, in the following, it has been adopted as varying between 0.05 and 0.20 MPa, that appears a reasonable range for existing masonries.

4.1. Voxel model validation

The effectiveness of the Voxel model (Fig. 1) to gather the main structural features of the Morris Island lighthouse is assessed in this section. In particular, its structural response is compared with the Smooth model (Fig. 1), which was assumed as reference model given the improved geometric representation and mesh discretization. Indeed, the jagged geometry of the Voxel model (Fig. 1) could appear, at a first sight, too poor for a reliable structural assessment, notably in the case of circular and tapering geometries as in the Morris Island lighthouse.

The outcomes of the Voxel model validation are shown in Fig. 2. Firstly, a natural frequency analysis is performed on both models by constraining the nodes at the base. As it can be observed in Fig. 2(a), the first four modal shapes of the Voxel and Smooth models appear very akin. This is also confirmed by very similar natural frequencies with a deviation $\leq$ 3% for the first four modes, see Fig. 2.

Secondly, pushover analyses with mass-and-height-proportional horizontal loads are performed on both models. A very good agreement between Voxel and Smooth models is observed both in terms of pushover curves and crack patterns, see, e.g., Fig. 2(b)-(c) for two non-perpendicular horizontal load directions (X axis (+X), and 45° from the X axis (+X+Y), i.e., the case in which the voxel discretization is more jagged). Accordingly, although the Voxel model has a simplified jagged geometry, its overall structural response appears substantially equivalent to the Smooth model. Therefore, this comparison serves as validation of the Voxel model, which is then used in the further analysis.

4.2. Nonlinear static analyses

In this section, nonlinear static analysis results are shown. Firstly, preliminary analyses are discussed in Section 4.2.1. Then, the use of static analyses for damage diagnostics is discussed in Section 4.2.2.

4.2.1. Preliminary analyses

Firstly, the influence of masonry tensile strength on pushover analyses is investigated (Fig. 3). Particularly, Fig. 3(a) shows the influence of tensile strength on pushover curves. As expected, base shear peaks increase while increasing f_t. More interestingly, a significant effect of f_t is observed in terms of crack patterns, see Fig. 3(b), where red colour indicates damaged states in tension. Indeed, the main cracking mechanism, while increasing the tensile strength from 0.05 MPa to 0.20 MPa, gradually turns from a pseudo-vertical cracking along with the full trunk of the structure to an inclined cracking in the bottom part of the structure.

Fig. 3 also highlights that the modelling of the indoor staircase (see Fig. 1 top right) has a non-negligible influence on pushover results. The indoor staircase has been modelled with rigid links where stiff steel beams are located, as these beams are the only points of connection between the staircase and the masonry structure. Particularly, Fig. 3(b) shows an example where the main cracking tends to be more vertically pronounced on the structure when considering the staircase. Accordingly, the model with indoor staircase is considered in the following analyses.

The Morris Island lighthouse leaning (approximately 1.5°) is clearly visible in Fig. 4, where the orthotropic top view of the point cloud is shown. Here, the possibility of leaning-induced damage in the lighthouse is preliminary investigated. Particularly, a foundation settlement idealized as a rigid rotation in the direction of leaning (in this case -X, i.e. a negative rotation around Y, Fig. 4) is monotonically applied considering the weakest masonry material (i.e. ft005) and geometric nonlinearity. As it can be noted in Fig. 4, the sole gravity does not induce any damage in the structure, suggesting that the leaning was not a main source of damage in the lighthouse. Indeed, the first appearance of cracks in the structure is due to a further rotation of the base of 6.44°. The progression of

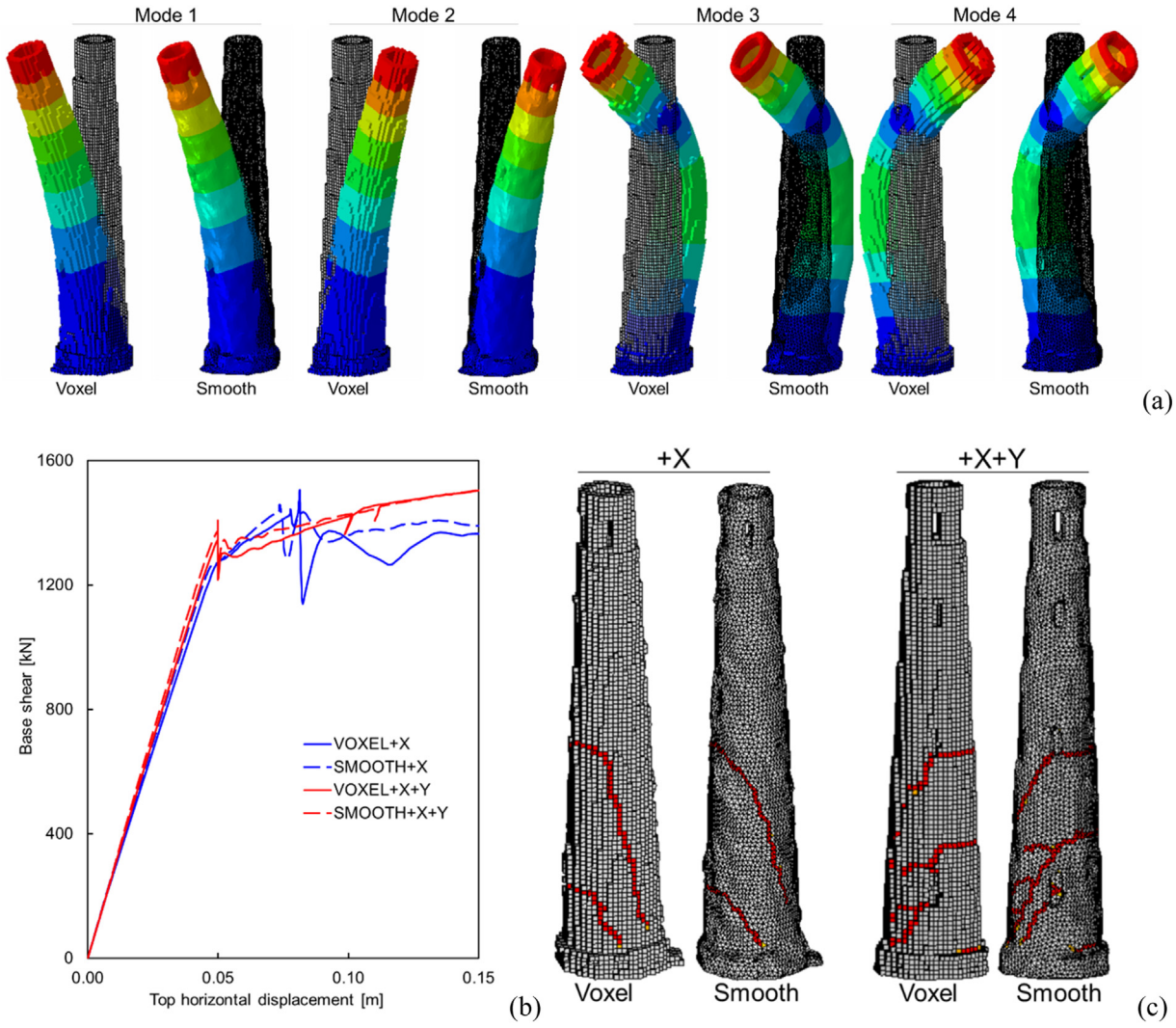

Fig. 2. Voxel model validation. (a) Natural frequency analysis results comparison: Mode 1 (Voxel frequency 1.29 Hz, Smooth frequency 1.31 Hz, deviation 1.5%), Mode 2 (Voxel frequency 1.33 Hz, Smooth frequency 1.35 Hz, deviation 1.5%), Mode 3 (Voxel frequency 4.84 Hz, Smooth frequency 4.97 Hz, deviation 2.6%), Mode 4 (Voxel frequency 4.85 Hz, Smooth frequency 5.00 Hz, deviation 3.0%). (b) Pushover curves comparison between Voxel and Smooth models (ft015) for two directions (+X and +X+Y). (c) Pushover analysis crack pattern comparison between Voxel and Smooth models for two directions (+X and +X+Y).

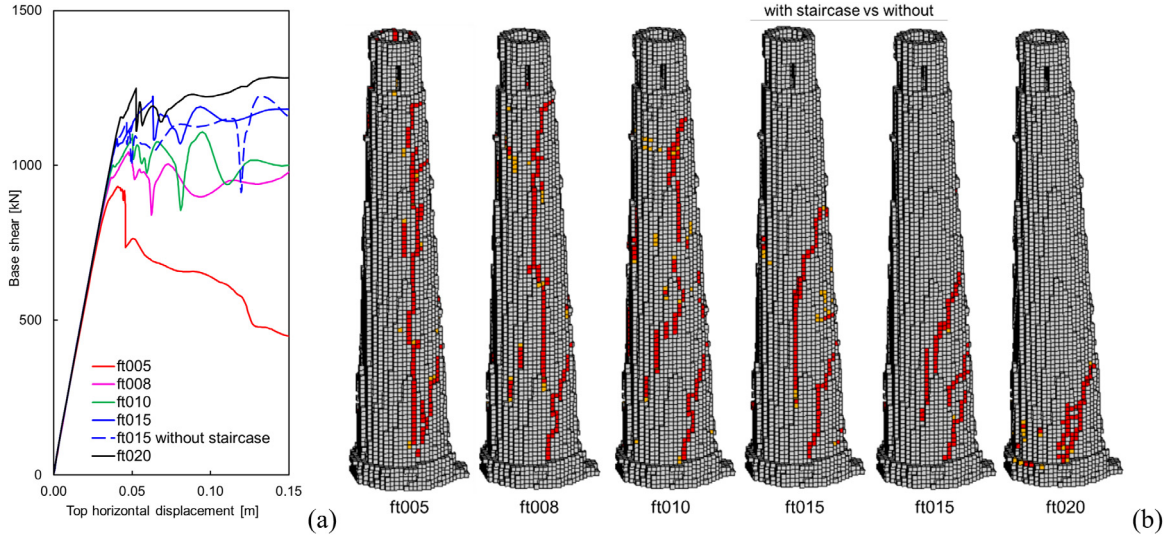

Fig. 3. Influence of masonry tensile strength on pushover analyses (case considered -X-Y). Five values of tensile strength f_t are considered: 0.05, 0.08, 0.10, 0.15, 0.20 MPa. The influence of the presence of the staircase is also shown for the case ft015. Nonlinear static analyses (pushover). (a) Influence of the masonry tensile strength on pushover curves. (b) Influence of the masonry tensile strength on the crack pattern.

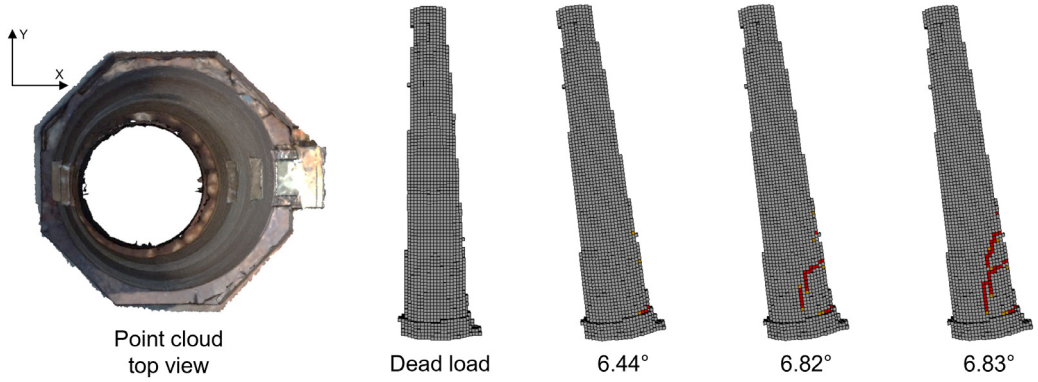

Fig. 4. Settlement (rigid rotation) in the direction of leaning (-X) considering the weakest masonry (ft005). From left: top orthotropic view of the point cloud; FE model subjected to dead load; first appearance of cracks due to a further rotation of the base of 6.44°; progression of the crack pattern at 6.82°; progression of the crack pattern at 6.83°.

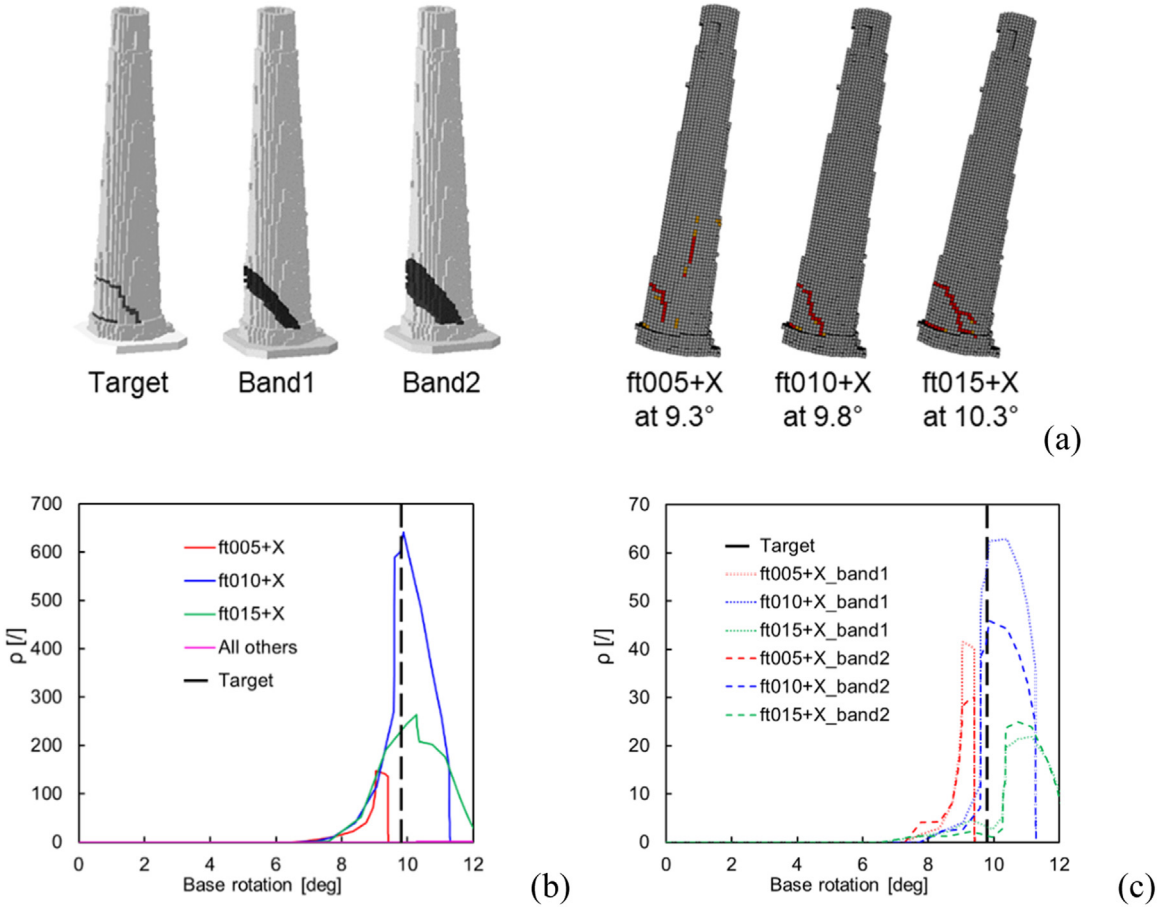

Fig. 5. Example of diagnostics of a settlement with 8 radial directions of testing. (a) From left: ideal target crack patter selected in agreement with the one obtained with ft010 and a settlement toward +X with a rigid rotation of the base equal to 9.8° (black elements show the Fissure zone, grey elements show the intact zone); band1 definition; band2 definition; crack pattern of ft005+X at 9.3°; crack pattern of ft010+X at 9.8°, and crack pattern of ft015+X at 10.3°. (b) Evolution of ρ along with the base rotation using the Fissure and Intact zone definition as in target. (c) Evolution of ρ along with the base rotation for band1 and band2.

the crack pattern, which reminds the Heyman's intuitions in [52], is shown in Fig. 4.

4.2.2. Damage diagnostics

Here, the damage diagnostics methodology is preliminary tested on a synthetic settlement-induced crack pattern to show the influence of the definition of Fissure and Intact zones on the crack pattern matching indicator ρ (Fig. 5). For this purpose, a numerically-obtained crack pattern is herein considered as actual crack pattern.

In particular, the target "actual" crack patter is manually selected according to the one obtained with ft010 and a settlement toward $+X$ with a rigid rotation of the base equal to 9.8° (Fig. 5(a)). In other words, dark elements in Fig. 5(a) are assumed as Fissure zone, while brighter elements are assumed as Intact zone. Then, 24 nonlinear static simulations are conducted by imposing base rigid rotations in 8 evenly spaced radial directions and, for each direction, by considering 3 values of tensile strength (i.e. ft005, ft010, ft015). The evolution of ρ along with the base rotation is shown in Fig. 5(b). As it can be noted, ρ values obtained in $+X$ analyses are

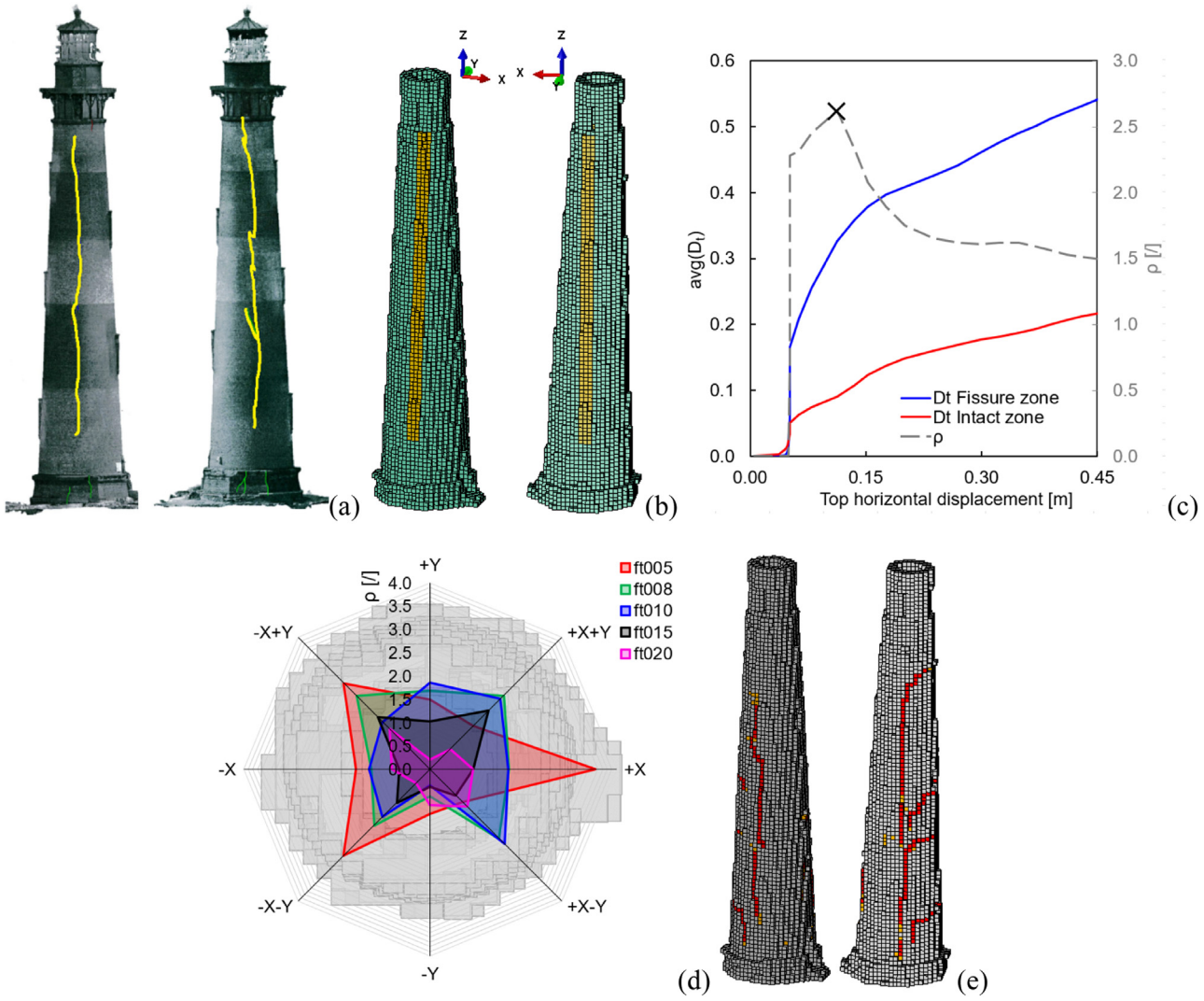

Fig. 6. Nonlinear static analyses (pushover). (a) Actual main crack pattern of the lighthouse (North front on left, South front on right, edited from [41]). (b) Definition of Fissure (yellow) and Intact (green) zones on the model (North front on left, South front on right). (c) Typical evolution of the average tensile damage variable in Fissure and Intact zones, as well as ρ, along with the pushover analysis. (d) Results in terms of ρ along with 8 radial directions of load application for 5 values of masonry tensile strength (from 0.05 MPa to 0.20 MPa). (e) Crack pattern of the best solution (+X ft005, North front on left, South front on right).

extremely higher (two order of magnitude) than the others. Particularly, ρ reaches the maximum value in the case ft010+X with a base rotation of 9.8°, which was indeed the target condition. The damage contour plots in correspondence of ρ peaks are shown in Fig. 5(a) for ft005+X, ft010+X, and ft015+X.

Furthermore, two other coarser choices of Fissure and Intact zones are considered, i.e. "band1" in and "band2" in Fig. 5(a), bearing in mind the same "actual" crack patter (i.e. the ideal target one). The evolution of ρ along with the base rotation for band1 and band2 is shown in Fig. 5(c). Also in this case, ρ reaches the maximum value in the case ft010+X with a base rotation very close to 9.8° for both band1 and band2.

Accordingly, the proposed methodology appears to be effective and not considerably influenced by the choice of Fissure and Intact zones. Finally, it should be stressed that ρ has a relative meaning, depending on the zone definition. Therefore, the comparison of ρ values obtained with different zone definitions has to be avoided.

Then, the damage diagnostics methodology is tested with pushover-like nonlinear static analyses on the actual main crack pattern of the Morris Island lighthouse (Fig. 6). The main actual crack pattern of the Morris Island lighthouse is composed of two large through-thickness pseudo-vertical cracks in North and South fronts, highlighted in yellow in Fig. 6(a). The definition of Fissure and Intact zones on the model, conducted in agreement with the actual crack pattern in Fig. 6(a), is shown in Fig. 6(b).

Mass-and-height-proportional horizontal loads are considered to statically simulate the seismic action. Horizontal loads are applied in 8 evenly spaced radial directions. For each load direction, 5 different values of tensile strength (ft050, ft080, ft010, ft015, ft020) are considered. Accordingly, the crack pattern matching indicator ρ is computed for each of the 40 load cases considered. A typical evolution of the average tensile damage variable in Fissure ($\bar{d}_F$) and Intact ($\bar{d}_I$) zones, as well as ρ, is shown in Fig. 6(c) along with the pushover analysis, i.e., along the top horizontal displacement. The peak value that ρ reaches along with the pushover analysis (marked with a cross in Fig. 6(c), represents the instant of the analysis that best fit the actual crack pattern.

Results in terms of peak ρ along with 8 radial directions of load application for the 5 values of masonry tensile strength considered are shown in Fig. 6(d). As it can be noted, ρ is significantly dependent on the load direction and on f_t. The best solution is obtained in the direction +X with ft005, see Fig. 6(e). The damage contour plots in Fig. 6(e) are indeed characterized by two main through-thickness pseudo-vertical cracks in North and South fronts. This

Table 1
Summary of best fits in pushover analyses with relative top horizontal displacements.

Direction	Tensile strength [MPa]	Top horizontal disp. [m]
+X	0.05	0.062
+X-Y	0.10	0.116
-Y	0.05	0.230
-X-Y	0.05	0.112
-X	0.05	0.133
-X+Y	0.05	0.060
+Y	0.10	0.545
+X+Y	0.08	0.130

outcome suggests that the actual crack pattern of the Morris Island lighthouse could have been indeed induced by an earthquake.

Beyond the direction of load, the proposed methodology is also able to roughly estimate the quality of the in-situ material (e.g. tensile strength) and the intensity of the load (in this case represented by the top horizontal displacement). The summary of the best fits for each direction of loading is presented in Table 1 in terms of tensile strength and top horizontal displacement. In particular, the best solution (i.e. ft005+X) is obtained for a low-quality material (i.e. low tensile strength) and for a small top horizonal displacement (Table 1), i.e. for a relatively small-intensity event. This aspect is further investigated in the next section through nonlinear dynamic simulations.

4.3. Nonlinear dynamic analyses

In this section, the damage diagnostics methodology is applied to the Morris Island lighthouse through the use of nonlinear dynamic analyses to simulate the effects of an earthquake. The incremental dynamic analysis (IDA) framework [53,14] is herein considered to investigate also the most likely peak ground acceleration (PGA) linked to the actual crack pattern of the structure.

To check the consistency of results, three different accelerograms are considered (from the Italian Accelerometric Archive, ITACA [54]) and scaled to 5 PGA values (i.e., 0.05 g, 0.10 g, 0.15 g, 0.20 g, 0.30 g). Particularly, the following accelerograms are considered [54]: (i) San Felice sul Panaro, Italy, May 29th, 2012 (SAN0 station, NS component, M_w 6.0), (ii) L'Aquila, Italy, April 6th, 2009 (AQA station, EW component, M_w 6.1), (iii) Croatia, March 22nd, 2020 (KOG station, NS component, M_l 5.3). Also in this case, 5 values of tensile strength and 4 radial directions are considered.

A total of 300 nonlinear dynamic analyses are performed by applying horizontal acceleration at the base nodes. The crack pattern matching indicator is computed for each analysis at the end of the simulation, adopting the Fissure and Intact zones as in Fig. 6(b). Results in terms of ρ are shown in Fig. 7 for all directions, PGAs, and tensile strength values considered. As it can be noted, higher values of ρ are observed in the X direction for any considered accelerogram, while the case with PGA equal to 0.05 g did not induce any significant damage in the Fissure zone in any case.

In particular, the best solution, characterized by a ρ significantly greater than all the other cases, is found to be X_ft005_ag010 in any case. The damage contour plots of X_ft005_ag010 are collected in Fig. 8 for the SAN0, AQA, and KOG. As it can be noted, although with some slight differences between each other, they are mostly characterized by 2 main through-thickness pseudo-vertical cracks in the North and South fronts, indeed in agreement with the actual crack pattern of the structure.

These outcomes confirm the insights of nonlinear static simulations, i.e., that the most likely load scenario which originated the crack pattern present in the Morris Island lighthouse is an earthquake with a predominant action along the X direction, considering a low-quality masonry material (i.e. ft005). Such low-quality material property appears plausible as the lighthouse is exposed

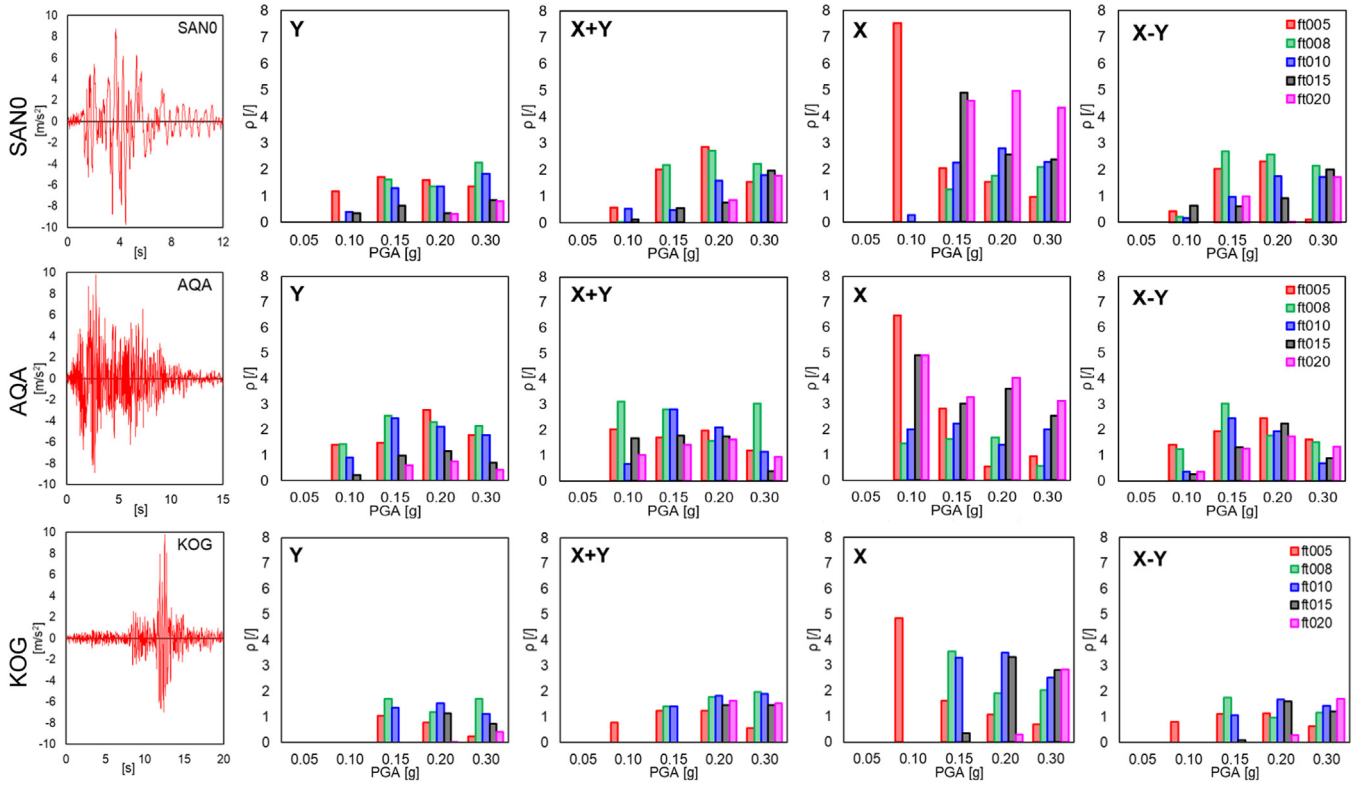

Fig. 7. Nonlinear dynamic analyses. Accelerograms on the left, histograms with values of ρ for several load directions, PGAs, and tensile strength values on the right. SAN0 accelerogram (top), AQA accelerogram (middle), and KOG accelerogram (bottom).

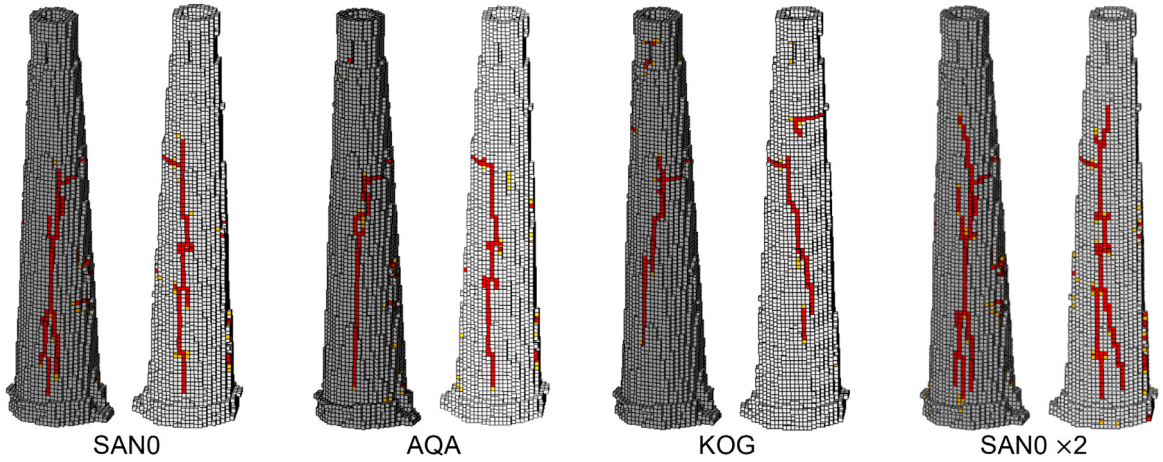

Fig. 8. Crack patterns of the best solutions, obtained in any case with X_ft005_ag010: SAN0, AQA, and KOG. SAN0 × 2 shows the crack pattern obtained by applying two subsequent dynamic analyses with X_ft005_ag010 and the SAN0 accelerogram.

to salt sprays which can induce accelerated material ageing (e.g., due to in-pore salt crystallization [55,56]). Furthermore, IDA-style nonlinear dynamic simulations can also estimate the intensity (i.e. PGA) of the most likely earthquake, in this case 0.10 g. This small-intensity event appears reasonable, as the largest earthquake ever recorded in the area is the 1886 Charleston earthquake, which has an epicentre about 15 km far from the Morris Island lighthouse and an estimated epicentral PGA equal to 0.33 g [40].

Once the most likely load scenario which originated damage is identified, it is also possible to identify the parts of the structure susceptible to further damage. By way of example, the lighthouse damaged by a X_ag010_SAN0 event (with ft005) is subjected to another identical seismic event. The resulting crack pattern is shown in Fig. 8. By comparing SAN0 with SAN0 × 2, a further extension and branching of the existing cracks can be observed, without inducing the collapse of the structure.

5. Conclusions

In this paper, a methodology for damage diagnostics in cultural heritage masonry structures based on numerical modelling has been proposed to quantitatively identify the most likely load scenario which originated the damage pattern present in the CHS.

Firstly, the rapid generation of the CHS numerical model from point clouds has been enhanced to also deal with non-comprehensive point clouds (e.g., related to external surfaces only) through an integration with off-site virtual tours.

Secondly, after the conduction of a number of nonlinear static and dynamic analyses on the generated model, a crack pattern matching indicator has been introduced to quantitatively identify the most likely load scenario which originated the damage pattern present in the CHS. Such indicator has been based on the comparison of numerical and actual crack patterns. Accordingly, the methodology allows the extraction of the model that reflects the current damaged state of the CHS, with the possibility to also identify in-situ material properties, event intensity, and the parts of the CHS susceptible to further damage.

The effectiveness of the methodology has been assessed on the historical Morris Island lighthouse in South Carolina (USA). The results, based on 24 pushover analyses and 300 nonlinear dynamic simulations, highlighted the consistency of the crack pattern matching indicator introduced. Particularly, the most likely load scenario identified to be the cause of the actual damage on the lighthouse appeared reasonable and consistent with the CHS history.

Acknowledgements

This project has received funding from the European Union's Horizon 2020 research and innovation programme under the Marie Sklodowska-Curie grant agreement No 101029792 (HOLAHERIS project, "A holistic structural analysis method for cultural heritage structures conservation"). The authors would also like to thank Rebecca Napolitano, Anna Blyth, Denis Blyth, and Save the Light, Inc. for sharing data and metadata on the lighthouse. Finally, Nicolò Lo Presti is gratefully acknowledged for providing technical support on the Cloud2FEM software.

Supplementary materials

Supplementary material associated with this article can be found, in the online version, at doi:10.1016/j.culher.2023.02.004.

Appendix

In this appendix, the mechanical properties of the masonry material assumed in the continuum model are shown. The isotropic continuum is characterized by a Young's modulus equal to 2500 MPa, a Poisson's ratio equal to 0.2, and a density equal to 1650 kg/m^3. Such properties have been adopted in agreement with the suggestions of the Italian Standards [57,58] for existing clay brick masonry.

To characterize the model proposed by Lee and Fenves [47], the following parameters are assumed according to [48]: angle of dilatancy equal to 10°, smoothing parameter of the Drucker-Prager type plastic potential equal to 0.1, ratio between biaxial and uniaxial compressive strengths equal to 1.16, and ratio at initial yield of the second stress invariant on the tensile meridian to the one on the compressive meridian equal to 0.667.

The model is finally characterized by uniaxial stress-strain relationships in tension and compression, assumed as bilinear and trilinear curves, respectively. In this study, the material tensile strength f_t is parametrically adopted, and the following values are considered: 0.05, 0.08, 0.10, 0.15, 0.20 MPa (ft050, ft080, ft010, ft015, ft020, respectively). The compressive strength has been set equal to 4.50 MPa, that is very close to the upper bound for solid clay brick masonry suggested in the Italian Standards [57,58]. Given that the structure is relatively recent, if compared with European heritage structures, it appears reasonable to adopt a compressive strength close to the upper bound. Furthermore, this is also in

Table 2
Uniaxial stress-strain and damage evolution relationships for the nonlinear continuum.

Compressive behaviour		
Stress [MPa]	Inelastic strain	d_c
4.50	0	0
4.50	0.002	0
0.45	0.008	0.9
Tensile behaviour		
Stress [MPa]	Inelastic strain	d_t
f_t	0	0
$f_t/10$	0.001	0.9

line with the first American Standard Building Code Requirements for Masonry [59]. Table 2 presents the properties defining the uniaxial stress-strain and damage evolution relationships, adopted in agreement with [48].

References

[1] W. Addis, Building: 3000 Years of Design Engineering and Construction, Phaidon Press, 2007.
[2] S. Mastrodicasa, Dissesti statici delle strutture edilizie, 1943.
[3] R.A. Galantucci, F. Fatiguso, Advanced damage detection techniques in historical buildings using digital photogrammetry and 3D surface anlysis, J. Cult. Herit. 36 (2019) 51–62.
[4] D. Loverdos, V. Sarhosis, Geometrical digital twins of masonry structures for documentation and structural assessment using machine learning, Eng. Struct. 275 (2023) 115256.
[5] V. Bosiljkov, M. Uranjek, R. Žarnić, V. Bokan-Bosiljkov, An integrated diagnostic approach for the assessment of historic masonry structures, J. Cult. Herit. 11 (3) (2010) 239–249.
[6] A. Anzani, L. Binda, A. Carpinteri, S. Invernizzi, G. Lacidogna, A multilevel approach for the damage assessment of historic masonry towers, J. Cult. Herit. 11 (4) (2010) 459–470.
[7] M. Mishra, Machine learning techniques for structural health monitoring of heritage buildings: a state-of-the-art review and case studies, J. Cult. Herit. 47 (2021) 227–245.
[8] A. Saisi, C. Gentile, Post-earthquake diagnostic investigation of a historic masonry tower, J. Cult. Herit. 16 (4) (2015) 602–609.
[9] F. Clementi, A. Formisano, G. Milani, F. Ubertini, Structural health monitoring of architectural heritage: from the past to the future advances, Int. J. Archit. Herit. 15 (1) (2021) 1–4.
[10] G. Fortunato, M.F. Funari, P. Lonetti, Survey and seismic vulnerability assessment of the Baptistery of San Giovanni in Tumba (Italy), J. Cult. Herit. 26 (2017) 64–78.
[11] N. Cavalagli, A. Kita, V.L. Castaldo, A.L. Pisello, F. Ubertini, Hierarchical environmental risk mapping of material degradation in historic masonry buildings: an integrated approach considering climate change and structural damage, Constr. Build. Mater. 215 (2019) 998–1014.
[12] P. Bamonte, G. Cardani, P. Condoleo, A. Taliercio, Crack patterns in double-wall industrial masonry chimneys: possible causes and numerical modelling, J. Cult. Herit. 47 (2021) 133–142.
[13] A. Kita, N. Cavalagli, M.G. Masciotta, P.B. Lourenço, F. Ubertini, Rapid post-earthquake damage localization and quantification in masonry structures through multidimensional non-linear seismic IDA, Eng. Struct. 219 (2020) 110841.
[14] A. Kita, N. Cavalagli, I. Venanzi, F. Ubertini, A new method for earthquake-induced damage identification in historic masonry towers combining OMA and IDA, Bull. Earthq. Eng. 19 (12) (2021) 5307–5337.
[15] A.M. D'Altri, V. Sarhosis, G. Milani, J. Rots, S. Cattari, S. Lagomarsino, E. Sacco, A. Tralli, G. Castellazzi, S. de Miranda, Modeling strategies for the computational analysis of unreinforced masonry structures: review and classification, Arch. Comput. Meth. Eng. 27 (2020) 1153–1185.
[16] R. Napolitano, B. Glisic, Understanding the function of bonding courses in masonry construction: an investigation with mixed numerical methods, J. Cult. Herit. 39 (2019) 120–129.
[17] D. Baraldi, A. Cecchi, Discrete approaches for the nonlinear analysis of in plane loaded masonry walls: molecular dynamic and static algorithm solutions, Eur. J. Mech. A. Solids 57 (2016) 165–177.
[18] K.M. Dolatshahi, M.T. Nikoukalam, K. Beyer, Numerical study on factors that influence the in-plane drift capacity of unreinforced masonry walls, Earthq. Eng. Struct. Dyn. 47 (6) (2018) 1440–1459.
[19] D. Addessi, E. Sacco, Nonlinear analysis of masonry panels using a kinematic enriched plane state formulation, Int. J. Solids Struct. 90 (2016) 194–214.
[20] L. Pelà, M. Cervera, P. Roca, An orthotropic damage model for the analysis of masonry structures, Constr. Build. Mater. 41 (2013) 957–967.
[21] B. Pantò, L. Macorini e, B.A. Izzuddin, A two-level macroscale continuum description with embedded discontinuities for nonlinear analysis of brick/block masonry, Comput. Mech. (2022) 1–26.
[22] F. Fraternali, A thrust network approach to the equilibrium problem of unreinforced masonry vaults via polyhedral stress functions, Mech. Res. Commun. 37 (2) (2010) 198–204.
[23] M. Angelillo, Static analysis of a Guastavino helical stair as a layered masonry shell, Compos. Struct. 119 (2015) 298–304.
[24] P. Block, J. Ochsendorf, Thrust network analysis: a new methodology for three-dimensional equilibrium, J. Int. Assoc. Shell Spat. Struct. 48 (3) (2007) 167–173.
[25] G. Torelli, D. D'Ayala, M. Betti, G. Bartoli, Analytical and numerical seismic assessment of heritage masonry towers, Bull. Earthq. Eng. 18 (3) (2020) 969–1008.
[26] C. Alessandri, M. Garutti, V. Mallardo, G. Milani, Crack patterns induced by foundation settlements: integrated analysis on a renaissance masonry palace in Italy, Int. J. Archit. Herit. 9 (2) (2015) 111–129.
[27] G. Milani, M. Valente, C. Alessandri, The narthex of the church of the nativity in Bethlehem: a non-linear finite element approach to predict the structural damage, Comput. Struct. (2017), doi:10.1016/j.compstruc.2017.03.010.
[28] M. Betti, M. Orlando, A. Vignoli, Static behaviour of an Italian Medieval Castle: damage assessment by numerical modelling, Comput. Struct. 89 (21–22) (2011) 1956–1970, doi:10.1016/j.compstruc.2011.05.022.
[29] R. Napolitano, B. Glisic, Methodology for diagnosing crack patterns in masonry structures using photogrammetry and distinct element modeling, Eng. Struct. 181 (2019) 519–528.
[30] R. Napolitano, B. Glisic, Hybrid physics-based modeling and data-driven method for diagnostics of masonry structures, Comput. Aided Civ. Infrastruct. Eng. 35 (5) (2020) 483–494.
[31] M. Korumaz, M. Betti, A. Conti, G. Tucci, G. Bartoli, V. Bonora, A.G. Korumaz, L. Fiorini, An integrated Terrestrial Laser Scanner (TLS), Deviation Analysis (DA) and Finite Element (FE) approach for health assessment of historical structures. A minaret case study, Eng. Struct. 153 (2017) 224–238.
[32] L. Kudela, S. Kollmannsberger, U. Almac, E. Rank, Direct structural analysis of domains defined by point clouds, Comput. Methods Appl. Mech. Eng. 358 (2020) 112581.
[33] A. Pesci, E. Bonali, C. Galli, E. Boschi, Laser scanning and digital imaging for the investigation of an ancient building: Palazzo d'Accursio study case (Bologna, Italy), J. Cult. Herit. 13 (2) (2012) 215–220.
[34] G. Castellazzi, A.M. D'Altri, G. Bitelli, I. Selvaggi, A. Lambertini, From laser scanning to finite element analysis of complex buildings by using a semi-automatic procedure, Sensors 15 (8) (2015) 18360–18380, doi:10.3390/s150818360.
[35] M. Pepe, D. Costantino, V.S. Alfio, A.G. Restuccia, N.M. Papalino, Scan to BIM for the digital management and representation in 3D GIS environment of cultural heritage site, J. Cult. Herit. 50 (2021) 115–125.
[36] G. Castellazzi, A.M. D'Altri, S. de Miranda, F. Ubertini, An innovative numerical modeling strategy for the structural analysis of historical monumental buildings, Eng. Struct. 132 (2017) 229–248, doi:10.1016/j.engstruct.2016.11.032.
[37] G. Castellazzi, N. Lo Presti, A. D'Altri, S. de Miranda, Cloud2FEM: a finite element mesh generator based on point clouds of existing/historical structures, Software X 18 (2022) 101099.
[38] D.W. Bostick, The Morris Island Lighthouse: Charleston's maritime Beacon, Arcadia Publishing, 2008.
[39] O.W. Nuttli, G.A. Bollinger, R.B. Herrmann, The 1886 Charleston, South Carolina, Earthquake: a 1986 Perspective, US Geological Survey, 1986.
[40] D.J. Elton, E.A. Marciano, Ground acceleration near St. Michael's Church during the 1886 Charleston, SC, earthquake, Earthq. Spectra 6 (1) (1990) 81–103.
[41] A. Blyth, R. Napolitano, B. Glisic, Documentation, structural health monitoring and numerical modelling for damage assessment of the Morris Island Lighthouse, Philos. Trans. R. Soc. A 377 (2155) (2019) 20190002.
[42] "Save the Light, Inc.," [Online]. Available: https://savethelight.org/.
[43] N. Lo Presti, G. Castellazzi, A. D'Altri, S. de Miranda, M. Azenha, S. Roggio, G. Bitelli, F. Ferretti, N. Rende and C. Mazzotti, From laser scanning to Finite Element and Building Information Modelling to support the structural assessment of historical buildings, *Submitted for pubblication,* 2023.
[44] R.K. Napolitano, G. Scherer, B. Glisic, Virtual tours and informational modeling for conservation of cultural heritage sites, J. Cult. Herit. 29 (2018) 123–129.
[45] D. Ferdani, B. Fanini, M.C. Piccioli, F. Carboni, P. Vigliarolo, 3D reconstruction and validation of historical background for immersive VR applications and games: the case study of the Forum of Augustus in Rome, J. Cult. Herit. 43 (2020) 129–143.
[46] G. Castellazzi, A.M. D'Altri, S. de Miranda, F. Ubertini, G. Bitelli, A. Lambertini, I. Selvaggi, A. Tralli, A mesh generation method for historical monumental buildings: an innovative approach, VII European Congress on Computational Methods in Applied Sciences and Engineering (ECCOMAS Congress 2016), 2016.
[47] J. Lee, G.L. Fenves, Plastic-damage model for cyclic loading of concrete structures, J. Eng. Mech. 124 (8) (1998) 892–900.
[48] A.M. D'Altri, F. Cannizzaro, M. Petracca, D. Talledo, Nonlinear modelling of the seismic response of masonry structures: calibration strategies, Bull. Earthq. Eng. (2021) 1–45.
[49] S. Cattari, D. Camilletti, A. D'Altri, S. Lagomarsino, On the use of continuum Finite Element and Equivalent Frame models for the seismic assessment of masonry walls, J. Build. Eng. 43 (2021) 102519.
[50] F. Messali, R. Esposito, G.J.P. Ravenshorst, J. Rots, Experimental investigation of the in-plane cyclic behaviour of calcium silicate brick masonry walls, Bull. Earthq. Eng. 18 (8) (2020) 3963 -399.

[51] G. Castellazzi, A.M. D'Altri, S. de Miranda, A. Chiozzi, A. Tralli, Numerical insights on the seismic behavior of a non-isolated historical masonry tower, Bull. Earthq. Eng. 16 (2) (2018) 933–961, doi:10.1007/s10518-017-0231-6.
[52] J. Heyman, Leaning towers, Meccanica 27 (3) (1992) 153–159.
[53] D. Vamvatsikos, C.A. Cornell, Incremental dynamic analysis, Earthq. Eng. Struct. Dyn. 31 (3) (2002) 491–514.
[54] L. Luzi, S. Hailemikael, D. Bindi, F. Pacor, F. Mele, F. Sabetta, ITACA (ITalian ACcelerometric Archive): a web portal for the dissemination of the Italian strong motion data, Seismol. Res. Lett. (2008).
[55] R.J. Flatt, Salt damage in porous materials: how high supersaturations are generated, J. Cryst. Growth 242 (3–4) (2002) 435–454.
[56] G. Castellazzi, A.M. D'Altri, S. de Miranda, H. Emami, L. Molari, F. Ubertini, A staggered multiphysics framework for salt crystallization-induced damage in porous building materials, Constr. Build. Mater. 304 (2021) 124486.
[57] *DM 17/01/2018. Norme tecniche per le costruzioni. Ministero delle Infrastrutture,* Rome, Italy *[Technical norms on constructions].*
[58] "Circolare n. 7 del 21 Gennaio 2019," Istruzioni per l'applicazione dell' «Aggiornamento delle "Norme tecniche per le costruzioni"» di cui al DM 17 gennaio 2018," 2019.
[59] American Standard Building Code Requirements for Masonry, National Bureau of Standandards Miscellaneous Publication M174, Washington D.C, 1944.